European Journal of Mechanics / B Fluids 86 (2021) 78–89

Contents lists available at ScienceDirect

European Journal of Mechanics / B Fluids

journal homepage: www.elsevier.com/locate/ejmflu

The mechanism of vortex bifurcation vis-à-vis axial switching in rectangular synthetic jets

Abhay Kumar [a,b], Arun K. Saha [b], Pradipta K. Panigrahi [b], Ashish Karn [a,*]

[a] Department of Mechanical Engineering, School of Engineering, University of Petroleum and Energy Studies, PO – Bidholi, Dehradun, Uttarakhand 248007, India
[b] Department of Mechanical Engineering, IIT Kanpur, UP 208016, India

ARTICLE INFO

Article history:
Received 30 November 2019
Received in revised form 3 September 2020
Accepted 1 December 2020
Available online 8 December 2020

Keywords:
Vortex bifurcation
Axial switching
Synthetic jet
Laser induced fluorescence
Laser Doppler Velocimetry

ABSTRACT

The present study investigates the vortex dynamics of the rectangular shaped synthetic jet and reports the occurrence of vortex ring bifurcation along with other reported modes such as axial switching and the vortex suction. The novel finding of vortex ring bifurcation of rectangular synthetic jets has been observed without any other mode of excitation except the periodic axial actuation. The experiments on synthetic jets have been conducted at different actuation frequencies and both qualitative and quantitative characterization of the flow structures has been carried out using Laser Induced Fluorescence (LIF) and Laser Doppler Velocimetry, respectively. LIF flow visualization provides insights into the size of the vortex and the vortex evolution with respect to time, enabling us to propose the flow physics behind the axial switching and the vortex bifurcation processes for rectangular synthetic jets. The proposed flow physics is then quantitatively evidenced by the time-averaged velocity measurements. Vortex splitting or bifurcation is found to occur in the minor axis plane of orifice and the divergence angle depends on the actuation frequency and average velocity of fluid expelled through the orifice in the forward stroke of diaphragm. In the case of occurrence of axial switching, a maximum of three axial switching events are observed before vortex breakup. Finally, by systematically carrying out experiments across a wide range of operational parameters, a narrow region corresponding to the vortex bifurcation has been identified on a *Reynolds Number–Strouhal Number* map, along with other modes such as axial switching regime and the vortex suction regime. Based on our measurements, a mechanism of vortex bifurcation vis-à-vis axial switching has also been suggested.

1. Introduction

The formation, propagation and interaction of vortex rings have been an active area of research due to its wide applications in nature and day-to-day life. Synthetic jets producing a train of large-scale coherent structures (vortex rings) with zero net mass flow rate have several practical applications, where the net momentum gain is used for controlling the flow or to achieve thrust [1]. The power supplied to the actuator is transferred to the fluid through oscillatory motion of a diaphragm resulting in vortex formation at the orifice exit. The vortex ring moves away from the exit plane under the influence of self-induced velocity and thus produces a jet called as synthetic jet [2]. The net mass transfer through the opening in one cycle is zero but there is a net transport of momentum to the ambient [3]. Therefore, the synthetic jet, also known as Zero Net Mass Flux (ZNMF) system finds its application in mixing [4,5], boundary layer control [6,7], propulsion [8–10], jet vectoring [11,12], cooling [13–16] and acoustics [17,18]. The vortex ring of the synthetic jet is affected by the flow field developed nearer to the jet exit. The near-field of the jet exit is characterized largely by a non-dimensional parameter Formation number, which is the ratio of slug length and the hydraulic diameter of the orifice. For a particular geometry of orifice, a threshold Formation number exists, beyond which any extra circulation generated by the ejecting shear layer ceases to flow inside the core region of the vortex ring. In such a case, the extra ejecting fluid gets pinched-off from the leading vortex ring and forms a trailing jet. For the similar phenomenon, another criterion was proposed by Utturkar et al. [19] using the order of magnitude analysis, where it was shown that for the successful formation of a vortex ring, the ratio of Reynolds number (Re) and the square of Stokes number (S), i.e. Re/S^2 must be greater than a particular constant value that depends upon the orifice geometry.

Among the two widely used orifice shapes having circular and non-circular geometries, the vortex ring ejected out of the non-circular orifice shows a differential induced velocity and thus

* Corresponding author.
E-mail address: akarn@ddn.upes.ac.in (A. Karn).

https://doi.org/10.1016/j.euromechflu.2020.12.002
0997-7546/

possesses greater instability as it travels downstream due to the existence of three-dimensional vortex dynamics such as the azimuthal distortions caused by the induction of the asymmetric coherent structures on its own, thus, increasing the fluid entrainment. Moreover, even among non-circular orifices, rectangular shape is of special significance since it offers passively improved mixing at the both the ends of the spectrum i.e. intensified large-scale entrainment due to axial-switching as well as enhanced small-scale mixing near corners and further downstream due to swift breakdown of vortex ring coherence.

The rectangular vortex ring shows broadly two types of vortex deformations: one that leads to axial switching of vortex ring and the other that causes bifurcation or splitting of vortex ring. Bifurcating jets, due to their augmented spreading angle as well as mixing In simple terms, vortex splitting is a phenomenon in which a single vortex gets stretched, leading to its disconnection and later reconnection to form two or more rings. Vortex bifurcation is a special case of such vortex splitting, when only two vortex rings are formed. The axial switching of rectangular vortex rings refers to the occurrence of a swap between major and minor axis of a rectangular vortex and has been reported by many researchers in the past [20–25]. Apart from these regimes, a vortex suction may also occur, where there is no distinct formation of vortex ring and the fluid ejected out from the orifice is sucked back partially or completely inside the cavity during the succeeding suction stroke. Yet, among these different modes, vortex bifurcation has been reported as the primary mechanism underlying the enhanced entrainment properties of non-circular jets relative to those of comparable circular jets. properties, are of particular interest for many practical applications [26]. However, it occurs only within a limited range of Strouhal number and Reynolds number [27,28]. Gohil et al. [29] reported that a round continuous jet could be bifurcated by simultaneously imposing helical and axial modes of forcing. On the other hand, other researchers (such as [30,31]) obtained the bifurcation in continuous jet or for a single vortex by combined effect of orifice shape and velocity of ejection. In this mode, the prime source of vortex splitting is variation in the self-induced velocity of vortex ring due to variation in curvature of nozzle or orifice. Oshima, Izutsu and Oshima [30] observed a partial bifurcation for a single vortex ring since the vortex ring collapsed just after the splitting and no isolated path for split vortex rings was observed.

However, in the case of single vortex rings, no perturbation exists in the environment before the formation of vortex rings and hence there is no influence of environment on the behavior of vortex rings. Further, in the case of a synthetic jet, the actuation frequency is an additional control parameter. Since in a synthetic jet, both the forward and the suction follow each other in a cyclic manner, the built up flow field of vortex ring continuously changes and influences the behavior of newly formed vortex ring. Therefore, the factors controlling the bifurcation process may behave differently in case of a synthetic jet. In an earlier work, we had investigated the flow physics and vortex behavior of rectangular orifice synthetic jets through LIF and Hot wire measurements and reported the occurrence of vortex bifurcation [23], although no clear understanding was gained as to what causes such bifurcation of rectangular orifice synthetic jets. Since the detailed mechanism of vortex bifurcation was not understood or discussed, a new series of experiments investigating the mechanism of vortex bifurcation was left as a future work. Hence, in the current study, we have explored the detailed mechanism of vortex bifurcation vis-à-vis axial switching by a systematic variation of Reynolds number (Re) and Strouhal number (St) and by measuring the time-averaged velocity through Laser Doppler Velocimetry measurements, as well as detailed flow-visualization in two orthogonal planes. Further, by systematically plotting the results of multiple sets of experiments on an *Re-St* map, we have located a narrow region where the process of vortex bifurcation occurs.

The current paper is organized in the following manner: Section 2 describes the experimental setup and methodology for both qualitative and quantitative measurements. In Section 3, experimental observations on dynamics of vortex bifurcation have been extensively dealt with in five subsections covering flow visualization, measurements on vortex size and evolution and the time-averaged velocity measurements. These measurements lead further to the description of the flow physics underlying axial switching and vortex bifurcation and finally regions pertaining to vortex bifurcation have been identified on a *Re-St* flow map. Subsequently, in Section 4, conclusions of the current study are enlisted.

2. Experimental setup and methodology

Fig. 1 shows a schematic of the experimental setup used in the current study, which includes a transparent water tank, a synthetic jet cavity with a diaphragm, an electromagnetic actuator, and a frequency controller. Fig. 1a shows a typical synthetic jet actuation system: It comprises of a mechanism to alter the volume of the chamber either through a flexible diaphragm or a piston. In our experiments, the actuation system consists of a cylindrical acrylic cavity, which has a convolute neoprene diaphragm at one end, and orifice at the other. Fig. 1b shows the dimensions of the cavity and the diaphragm. It should be noted that the dimensions of the cavity, diaphragm, the water tank and the positioning of the orifice has been kept identical to the previously reported study [23]. The actuator lies at a distance of 250 mm from the bottom of the tank as well as from the free surface, and the orifice of hydraulic diameter 12 mm (hydraulic diameter) yields a low blockage ratio of 2.4%. The dimensions of the rectangular orifice are 7×14 mm^2 with an orifice thickness of 3 mm. The orifice cross-section, the axis notation and the separation distances between the two counter-rotating vortices coming out of the orifice in XZ plane (H_W) and in XY-plane (H_B) are shown in Fig. 1c.

Laser-Induced Fluorescence (LIF) has been used for flow visualization, along with an articulated arm and the sheet optics to direct the laser sheet within the water tank, as presented in Fig. 1d. A 4 W continuous wave Ar-Ion Laser is used as the light source and the flow images are captured at 30 fps at a resolution of 600×1280 pixels. The LIF images are acquired at different instants of time in major and minor axis planes for a qualitative study. A concentrated solution of Fluorescein sodium is used as the dye for visualization purposes. The actuation process is begun after the dye is injected slowly and carefully and the initial few cycles are captured. The vortex core location obtained from LIF images has an uncertainty of 6.2%.

The velocity measurements in the streamwise and cross-streamwise direction are carried out using a five-beam Laser Doppler Velocimetry (LDV) probe as presented in Fig. 1e. Two colors of beams green (514.5 nm) and blue (488 nm) are used for measuring the two components of velocity. The waist diameter and length of the measuring volume are equal to 145 μm and 4.2 mm for 514.5 nm laser beam and 137 μm and 2 mm for wavelength 488 nm laser beam. The fringe spacing and number of fringes are 7.47 μm and 19, respectively for a wavelength 514.5 nm. Similarly, for a wavelength of 488 nm, these are equal to 3.54 μm and 39, respectively. Since there are three different optical media such as air, Perspex, and water in the current experiments, the necessary correction in traverse movement is given. Hollow glass spheres coated with silver in the diameter range of 8 μm–12 μm are used as external flow seeding particles.

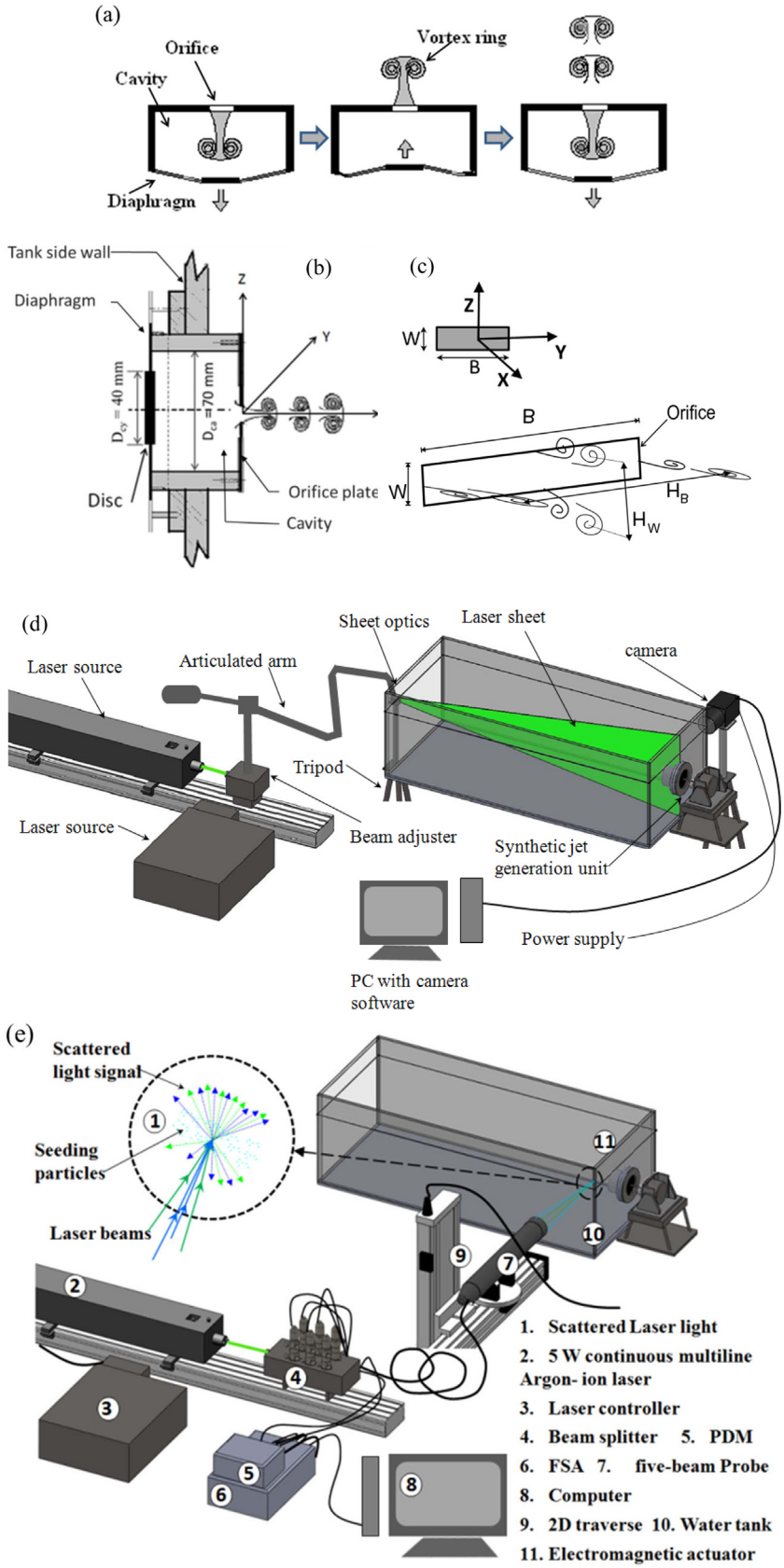

Fig. 1. (a) Schematic of the synthetic jet actuator, (b) Cross-sectional view of the orifice, orifice cavity and diaphragm, (c) the nomenclature of orifice orientation, axis notations and separation distance between the core of counter rotating vortices (d) Schematic of the experimental set-up for LIF imaging, and (e) Schematic of the experimental set-up for five-beam Laser Doppler Velocimetry (LDV) measurements.. (For interpretation of the references to color in this figure legend, the reader is referred to the web version of this article.)

At each point, the velocity data is sampled over a minimum 60 operational cycles, and an arithmetic mean is obtained. A maximum fluctuation of ± 3.7% around the mean is observed in the measured velocity components considering uneven sampling.

In general, the physics of the synthetic jet is characterized by the physical parameters such as hydraulic diameter of the orifice (D_h), the synthetic jet exit velocity during the forward stroke (U_o), actuation frequency of synthetic jet (f), suction stroke time (T_s), ejection stroke time (T_e), slug length (L), the orifice cross-sectional area (A_0) and volume of fluid expelled from orifice (V_D) which is identically expressed as volume displaced by forward stroke of diaphragm (V_D). The total cycle time (T) is given as the sum of suction and ejection stroke time as $T = T_s + T_e \approx 2T_e$, and thus the actuation frequency is given by $f = 1/2T_e$. These parameters are commonly expressed using the three dimensionless groups: Reynolds number, $Re = U_o D_h/v$; Strouhal number, $St = fD_h/U_o$ and the formation number, $Fn = L/D_h$ which is a normalized stroke length. The slug length L is given as $L = V_D/A_o$ and the synthetic jet exit velocity is determined by $U_o = V_D/A_o T_e$, or $U_o = 2fL$. Further, for the determination of slug length, V_D is estimated using cavity inner diameter (D_{ca}), disk diameter (D_{cy}) and amplitude of oscillation (Δ) as given by Mohseni [32]: $V_D = \pi \Delta \left(D_{ca}^2 + D_{cy}^2\right)/8$, where Δ is measured by an accelerometer in our experiments. The uncertainty in fluid volume ejection, formation number (L/D_h) and Reynolds number equals 3.6%, 3.6% and 3.7%, respectively.

3. Results and discussion

Experiments are conducted on a rectangular orifice of aspect ratio two at a range of actuation frequencies in the range of 1–3 Hz, and the resulting flow physics is recorded using both qualitative (LIF) and quantitative (LDV) measurements as the LIF images are not free from attenuation and stagnant dye illumination, and thus the captured images being considered belong to the initial few cycles. The resulting measurements provide an insight into the flow physics involved in axial switching and vortex bifurcation. An orifice of aspect ratio two is chosen for these experiments based on the information acquired from prior reports in the literature. Table 1 below presents the details of all the experiments conducted at which bifurcation or axial switching phenomenon has been observed.

3.1. Flow visualization

Fig. 2 shows the LIF images of vortex ring bifurcation at actuation frequency of 1, 2 and 3 Hz. The LIF images of vortex ring are captured from both the *XZ*-plane (or minor axis plane) and the XY-plane (i.e. the major axis plane). It may be pointed out that although the reported images are exactly not at the same instant of time for both the views, care has been taken to ensure that the number of cycles elapsed since the initiation of the synthetic jet is kept same for different cases of actuation frequency.

Fig. 2a shows the splitting of vortex ring for Case I, where the vortex ring bifurcates in the *XZ*-plane and moves approximately at an angle of 62° with each other in the downstream direction. Fig. 2b shows the vortex splitting with splitting angle equal to 46° for Case II with some portion of vortex ring left at the center during the splitting, forming a Ψ-shape of flow structure. In top view, the converging angles of counter rotating vortices from orifice exit to the point of merging are approximately 56° and 40° for Case I and Case II, respectively. Further, as illustrated in Fig. 2c for Case III, the split vortex rings show a smaller splitting angle equal to 34° with no clear or distinct splitting being observed in the side view images. Here, the process of bifurcation initiates but before the completion of bifurcation or splitting, the vortex ring breaks into smaller vortices and moves all around randomly. Oshima et al. [30] reported that at the point of vortex reconnection (see Fig. 2a), counter rotating vortices comes closer by canceling the outer part of adjacent vortex filament. At the same time, a breakdown is initiated at the crosslinking region, generating abrupt turbulence in the vortex filament. These turbulence structures propagate around the remaining vortex tube from and tear apart the vortex ring into further tiny vortical structures, and thus the bifurcation phenomenon is not observed. In all the three cases of bifurcation — Case I, II and III, the vortex rings either split or show a tendency to split just after the first axial switching in the minor axis plane of the orifice. Such splitting of vortex rings has been reported by Kiya, et al. [33] with the help of numerical simulations and experimental data. They showed the bifurcation of single pseudo-elliptical vortex ring in both planes (minor and major axis plane) for aspect ratios in the range of 2 to 20. They observed four different patterns as, pseudo-periodic axial switching for 2 < AR < 4, axial switching followed by vortex splitting in the minor axis plane for 5 < AR < 8, vortex ring splitting without axial switching in the major axis plane for 8.9 < AR < 11 and, vortex ring splitting into three distorted vortex rings without experiencing any axial switching for large aspect ratios in the range of 11< AR < 20. Vortex splitting in the major axis plane has also been reported by Auerbach and Grimm [34], based on the divergence or convergence of the counter rotating vortices in the captured images. Although the prior studies have indicated that bifurcation can occur in both the minor or major planes, in the present study, bifurcation was found to occur only in the minor axis plane and no sign of bifurcation is observed in the major axis plane of the orifice for all the considered cases.

However, the trend of the vortex ring splitting obtained in our experiments for a rectangular synthetic jet ejected out of an orifice of aspect ratio two is in good agreement with the results of Kiya et al. [33] for a single pseudo-elliptical vortex ring at an identical orifice aspect ratio. Since, subsequent to the first axial switching, the major axis of vortex ring becomes minor and vice-versa, the initially shorter side of the vortex rings switches in the minor axis plane (*XZ*-plane) of the orifice. Therefore, the vortex reconnection and splitting events occur in the *XZ*-plane, perpendicular to the longer side of orifice. Another noteworthy observation is the location of the vortex crosslinking, highlighted by the dots in the top view of LIF images (see Fig. 2a, 2b). This location varies between $X/B = 1.5$ for Case I to $X/B = 2.5$ for Case II. It indicates that the point of the vortex splitting is not fixed and may vary depending on other experimental parameters. Further, the top view in the LIF images (see Fig. 2) also present an interesting aspect of the synthetic jet flow physics — the occurrence of partial vortex leap forging, whereby the newly formed counter rotating vortices penetrate inside the leading vortex ring and moves ahead due to a velocity difference. In this process, the vortex rings are squeezed in the beginning and are finally consumed inside the envelope of previous rings. Careful examination of the video corresponding to the LIF images in the *XY*-plane suggests that the piercing action of the converging vortices pushes the envelope of fluid away from the synthetic jet centerline in the region between $X/B = 0.5$ to 1.5 during advection. As the counter rotating vortices move ahead, the envelope moves down to fill the gap. This cycle repeats and the envelope oscillates in *Y*-direction for each passage of counter rotating vortices as shown clearly in Fig. 2a and 2b.

Fig. 3 presents the LIF images of the synthetic jet at identical actuation frequencies of 1, 2 and 3 Hz, but with an increased diaphragm displacement. As Fig. 3 shows, the synthetic jet experiences an axial switching instead of vortex ring bifurcation in these cases. The vortex rings are isolated and the trailing jet is negligible for Case IV, but a small amount of trailing jet

Table 1
Details of the experimental conditions.

Cases	Actuation frequency (f) Hz		Reynolds number (Re)	Strouhal number (St)	L/D_h	Remark
	Actual	Round-off				
I	1.02	1	275	0.33	1.51	
II	1.60	2	1101	0.13	3.83	Bifurcation or vortex splitting
III	2.56	3	1309	0.17	2.94	
IV	1.02	1	625	0.15	3.42	
V	1.60	2	1348	0.10	4.69	No bifurcation or axial switching
VI	2.56	3	2038	0.11	4.57	

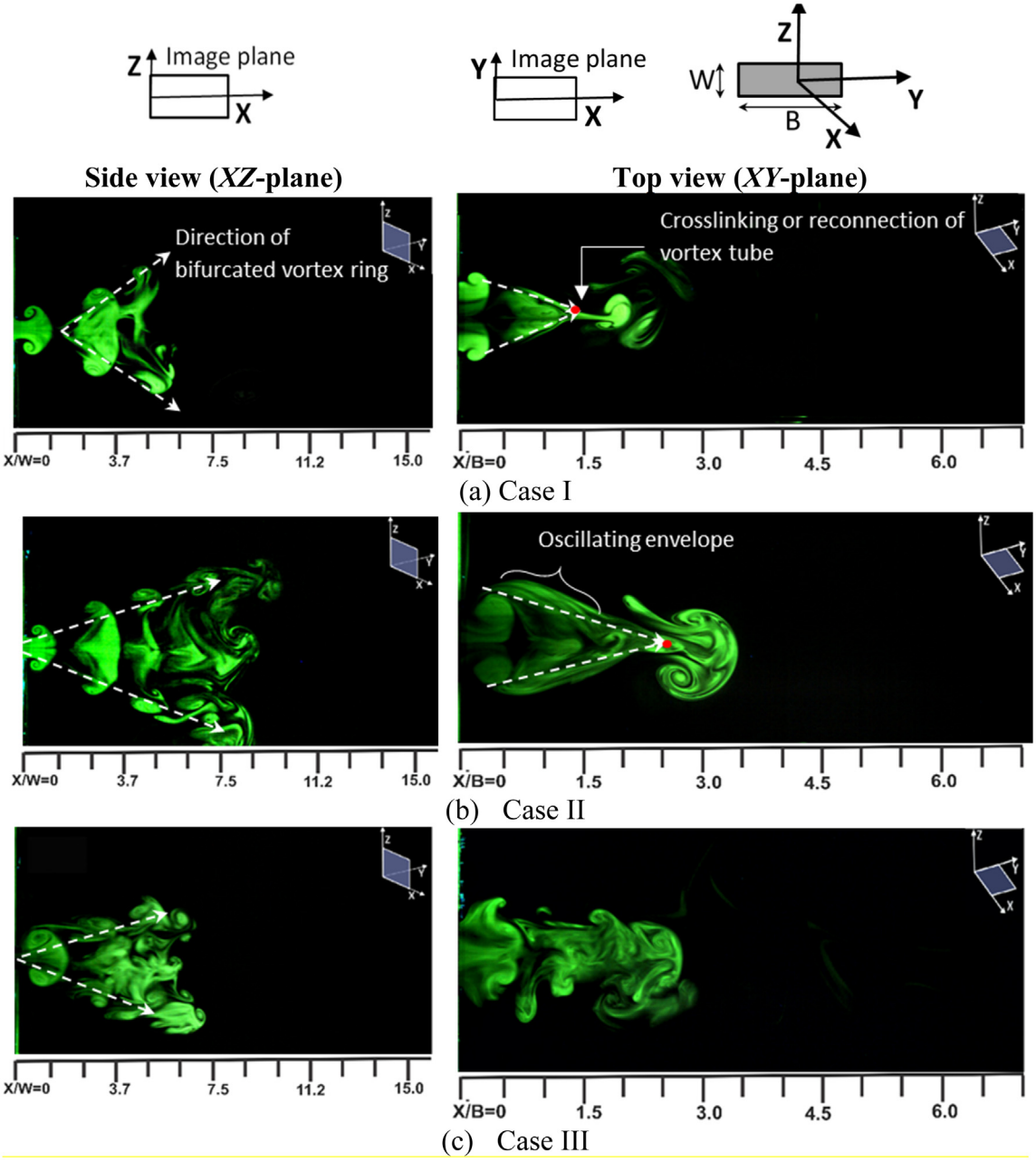

Fig. 2. Flow visualization images of synthetic jet in XZ-plane (side view) and in XY-plane (top view) for bifurcation cases: (a) Case 1, (b) Case II and (c) Case III. It may be noted that the images are not exactly at the same instant of time with reference to the actuation cycle.

forms for Case V, which interacts with the following vortex rings. The increased actuation frequency from 1 to 2 Hz decreases the spacing between the vortex rings and increases their interaction, which can be seen from the early breakdown of the vortex ring. In Case VI, the images in both the planes show a significant amount of trailing jet.

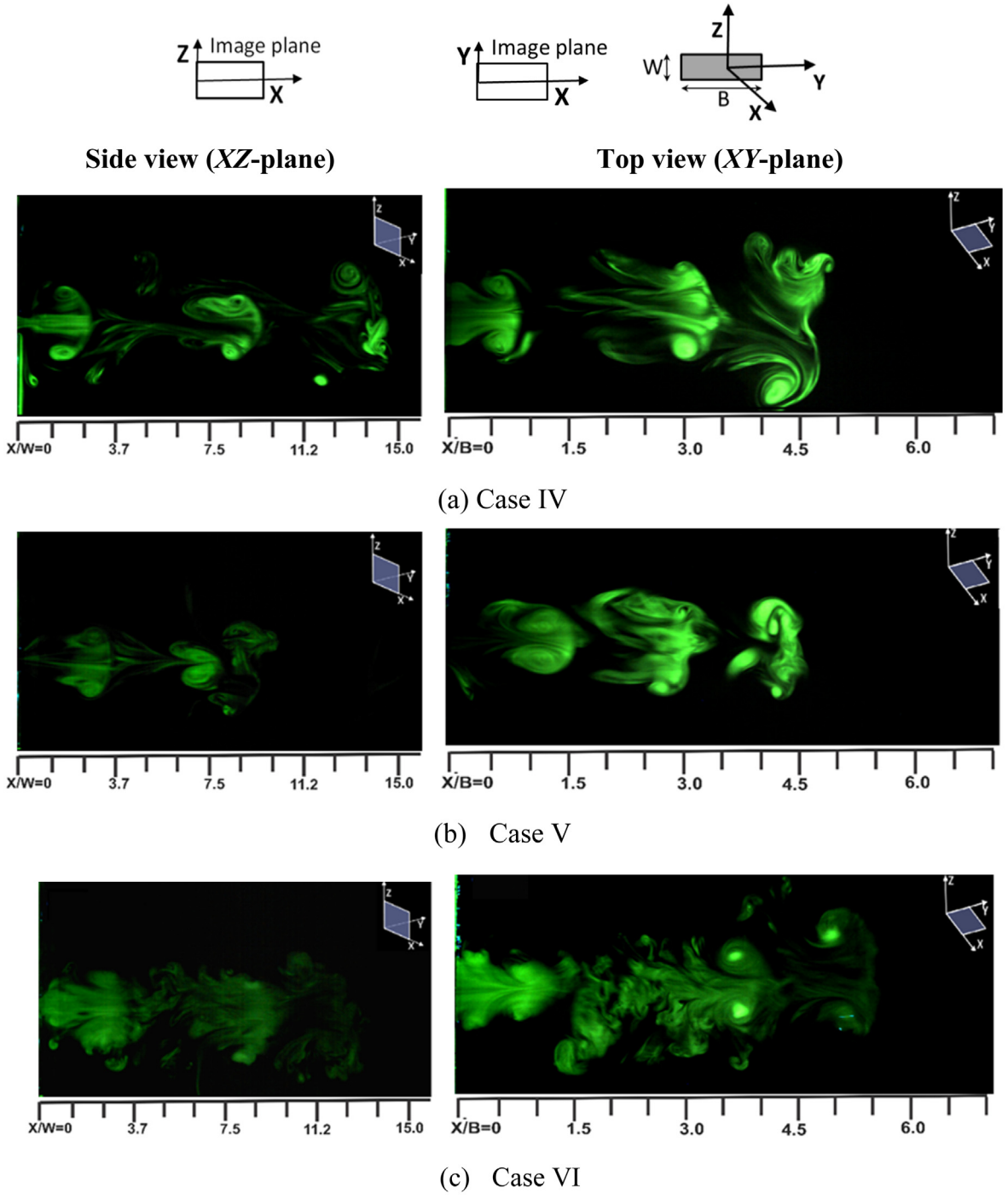

Fig. 3. LIF visualization of the synthetic jet in the side view (XZ-plane) and in the top view (XY-plane) for no-bifurcation cases: (a) Case IV, (b) Case V and (c) Case VI. It may be noted that the images are not exactly at the same instant of time with the reference to the actuation cycle.

3.2. Size of the vortex

To explain the vortex growth and behavior of the vortex ring, the vortex size variation has been studied extensively. The trajectory of the counter rotating vortices is studied from the series of LIF images in *XZ* and *XY*-plane and is presented in Fig. 4. The figure shows that the formation of trailing jets is also observed in some cases but the global flow pattern largely depends on the vortex dynamics of the leading vortex rings. Hence, the separation distance between the cores of counter rotating vortices of leading vortex ring provides useful information about the formation and evolution of the synthetic jet. To properly characterize the size of the vortex, the separation distances in the spanwise (i.e. the XY plane) and the vertical directions (i.e. the XZ plane) have been marked as H_B and H_W, respectively as shown in Fig. 4. Next, the measured values of separation distances are presented in both time and space domain for all the six cases. In the bifurcation cases, I, II and III shown in Fig. 4a, the separation distance between the oppositely rotating vortices in both the orthogonal planes follow the same trajectory in time domain before the first axial switchover. After the first axial switchover, the initially shorter side becomes longer and vice versa between $t/T = 0.6$ to 0.9 in the time domain corresponding to $X/W = 1$ in downstream

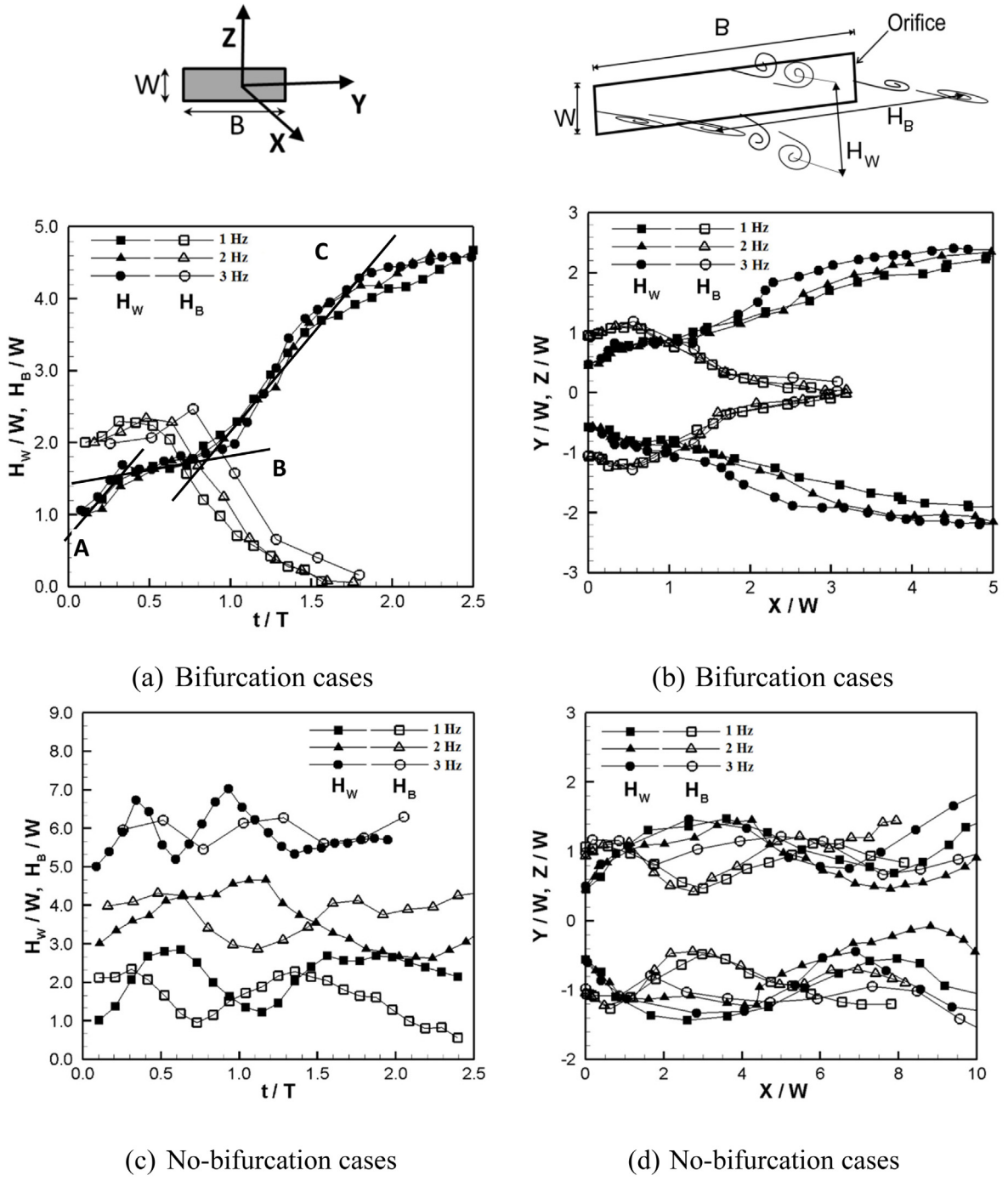

Fig. 4. (a) Time evolution of separation distance between the cores of counter rotating vortices for bifurcation cases (b) location of cores in XZ and XY planes for bifurcation cases, (c) Time evolution of separation distance between the cores of counter rotating vortices for non-bifurcation cases, and (d) location of cores in XZ and XY planes for non-bifurcation cases. (*The values of H_B and H_W are displaced along the Y axis by step size equal to two for clarity.)

direction. The trajectory of counter rotating vortices in the *XZ*-plane for bifurcation cases have three distinct regions represented by three straight lines as shown in Fig. 4a. The regions are: (i) duration in which shear layer rolls into a vortex ring (line-A), (ii) duration after first axial switching when the longer side of vortex ring interconnects and then splits (line-B) and (iii) the split vortex rings moving at an angle (line-C). Smaller slope of line-B indicates that during the vortex reconnection and the splitting period, the size of vortex ring in bifurcation plane does not change. Once the splitting is completed, the split vortex rings moves at an angle to each other, as evident from a greater separation distance between the upper and the lower vortex rings. The vortex size variation for the bifurcation cases I, II and III follow the same trajectory in downstream direction in both the orthogonal planes, as illustrated in Fig. 4b. The opposite spinning vortices in the *XY*-plane drift towards the center (see Fig. 2) and vanish at $X/W = 3$, whereas the vortices are present up to $X/W = 5$ in the *XZ*-plane.

In general, the rectangular shaped vortex ring expands in the direction of minor axis and contracts in the direction of major axis due to differences in its self-induced velocities in the two directions. Shortly thereafter, minor and major axes switch, and once this first switchover is completed, a second switchover is between the axes is also observed after a while. However, this

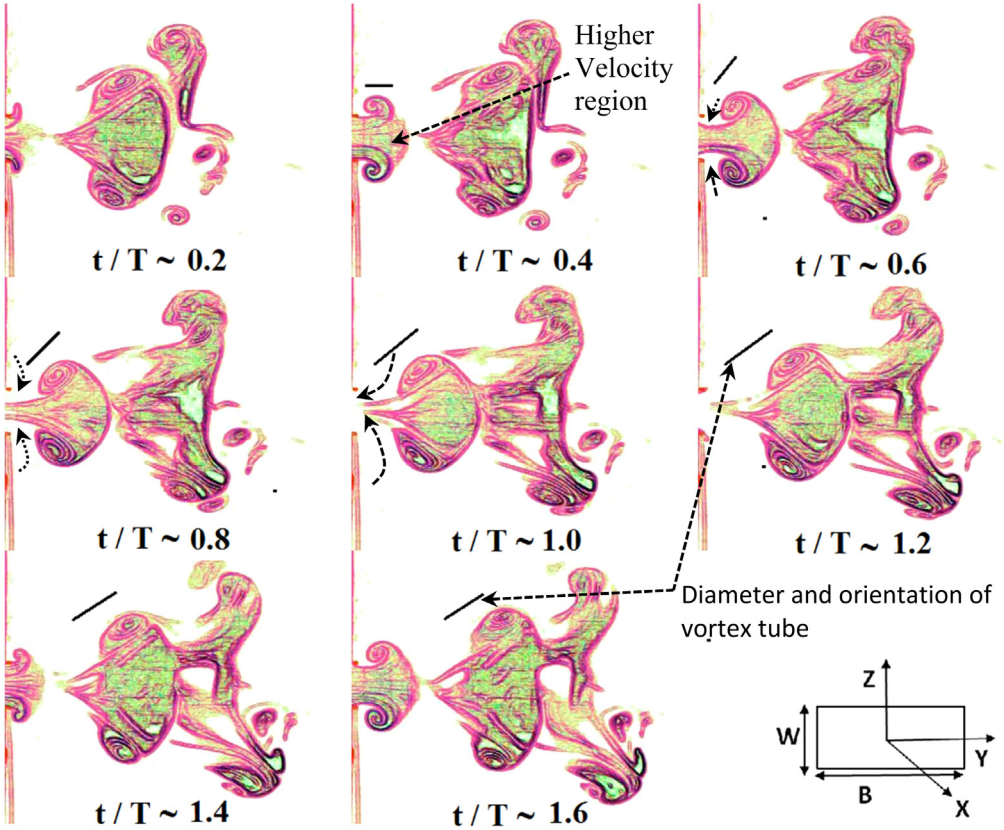

Fig. 5. Sequence of LIF images showing vortex evolution and bifurcation process at different instants of time in the *XZ*-plane for Case I. Colors are introduced to enhance visibility of LIF images.. (For interpretation of the references to color in this figure legend, the reader is referred to the web version of this article.)

process of axial switching cannot continue indefinitely. The vortex size expansion, entrainment of the surrounding fluid, growth of core instability and subsequent reduction in velocity restricts the number of total axial switching before the vortex breakdown. A maximum of three axial switching events have been reported for elliptical jets by Hussain and Husain [35]. They also reported that the third axial switching is usually faint and may not be easily detectable. Similar findings were also reported by Ho and Gutmark [36], who observed maximum three axial switching in an elliptical nozzle of aspect ratio two for a free air-jet.

A maximum of three axial switching is observed from the trend (H_B and H_W switching their value relative to each other) of counter rotating vortices in Fig. 4c and 4d for Case IV, V and VI. The trajectory of counter rotating vortices shown in Fig. 4d, shows that the size of both the minor and major axis of vortex ring is equal at $X/W \sim 1$. However, the location of the first axial switch-over vary significantly for Case VI in comparison to Case IV and V which is likely to be linked with the strong trailing jet observed for the former case, as evident from Fig. 4c.

3.3. Vortex evolution

The instantaneous images of vortex evolution and bifurcation process are shown in minor and major axis planes in Figs. 5 and 6, respectively. The cross-sectional view of vortex tube appeared in LIF images continuously changes its shape during its evolution near the orifice exit due to variation in self-induced velocity initiated by the orifice curvature. Figs. 5 and 6 presents the qualitative information on vortex evolution in both the *XY* and *XZ* planes at different times. At $t/T = 0.4$ in Fig. 5, the fluid ejected from the orifice center is ahead than the fluid curling to form the vortex tube near the orifice wall. However, at the same instant of time in Fig. 6, the fluid ejected at the orifice center lags behind the fluid at the orifice wall. Another interesting observation is that the rolling of shear layer to form the vortex tube in *XY*-plane is weaker than that of the curling of shear layer in *XZ*-plane at the same time. The differences in curling radius of the vortex tube formation in *XY* and *XZ*-plane forms vortex ring of a varying tube radius and velocity. As a result, the axis of the vortex tube gets stretched and tilted (indicated by small straight lines drawn just above the upper counter rotating vortices) in the *XZ*-plane and contracts in the *XY*-plane. As shown in Fig. 4a, the region on line-A that overlaps with Line-B corresponds to this contraction and stretching phenomenon where the vortex rolls to form counter rotating vortices. At the end of the forward stroke, when the vortex ring detaches itself from the orifice and moves downstream and nearly at the same instant, the backward stroke of the diaphragm initiates the suction stroke. Hence, the fluid moving towards the orifice cavity squeezes the newly formed vortices at its rear end and changes the shape and orientation of vortex tube as shown in Fig. 5 at $t/T \sim 0.6$. Due to changes in orientation and shape, the counter rotating vortices moves away from the synthetic jet centerline in *XZ*-plane in Fig. 5 and comes closer in *XY*-plane at $t/T \sim 0.8$ and 1.0 in Fig. 6. In the *XY*-plane, H_B decreases continuously with time and the left over portion of the former vortex rings creates an envelope over the newly formed vortices and squeezes it along the synthetic jet centerline. This physical phenomenon corresponds to the region on line-B that overlaps with line-C, where H_W does not changes significantly. The contraction of counter rotating vortices at $t/T = 1.2$ to 1.6 in Fig. 6 leads to vortex tube reconnection in *XY*-plane and bifurcation in *XZ*-plane as seen in Fig. 5 (line-C in Fig. 4a). The sequence of images reveals that the thickness of envelope increases initially, but remains unchanged with the progression of time.

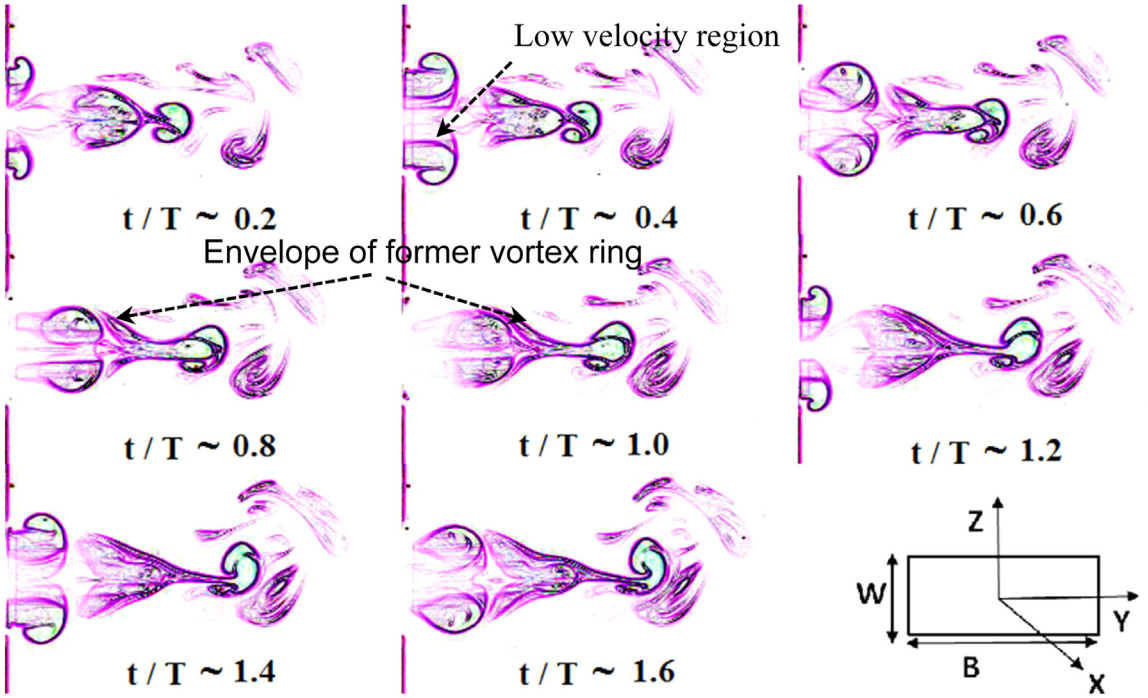

Fig. 6. Sequence of LIF images showing vortex evolution and bifurcation process at different instants of time in the *XY*-plane for Case I. Colors are introduced to enhance visibility of LIF images.. (For interpretation of the references to color in this figure legend, the reader is referred to the web version of this article.)

Based on the above experimental observations, the schematic of axial switching and bifurcation of rectangular shape vortex ring has been shown in Fig. 7. At the orifice exit, the shorter sides of vortex tube are labeled as S_1 and S_2 and longer sides are labeled as l_1 and l_2. The vortex ring experiences axial switching or splitting depending on the flow conditions imposed on it. As soon as the vortex ring detaches itself from the orifice, the shorter side (S_1, S_2) moves swifter than the longer side (l_1, l_2). The differences in the velocities along two orthogonal directions produce strain within the vortex ring. However, a greater strain rate results in the shorter side of vortex ring that makes it move towards the vortex center and pushes the longer side away from the center. If the vortex ring has enough energy and a comparatively lower velocity difference between the shorter and the longer side, the two edges exchange roles, i.e. the initially shorter edge becomes elongated, whereas the initially longer edge contracts and becomes short. This transition is depicted in Fig. 7a, where the shorter side moves ahead towards the vortex center pushing the longer side away from the orifice (shown by arrowheads) such that the shorter side S_1, S_2 becomes longer, and longer side l_1, l_2 becomes shorter. This process continues until the vortex breakdown, as also evident from the oscillating variation of H_w and H_B, as shown in Fig. 4c and 4d.

A slightly different physical mechanism is observed in the event of vortex bifurcation, as shown in Fig. 7b. The shorter sides of vortex ring (S_1, S_2) approach each other very closely as compared to the axial switching cases, leading to the vortex interconnection (see separation distance H_B of counter rotating vortices in Fig. 4b and corresponding images in Fig. 5). The envelope formed from previously ejected vortex rings (Fig. 6) also supports the interconnection of vortex tube, which is also called as *crosslinking* or *connect-and-cut process*. The crosslinking of vorticity is a cut and connect process in which the core deformation and stretching is followed by annihilation and bridging, which is completed by threading and splitting [37]. Similar observations have been made in the work of Yao and Xungang [38], which report that the opposite-signed vorticity (here counter rotating vortices of vortex ring) inside the contact zone gets canceled out by viscous cross-diffusion. These canceled vortex lines of vortex tube gets connected with their counterpart and forms isolated vortex rings. Thus, the process of vortex splitting is the result of crosslinking of vortex tube.

3.4. Time-averaged velocity measurements

The velocity components measured using Laser Doppler Velocimetry along the synthetic jet centerline is shown in Fig. 8. The filled and gray symbols represent the cases of axial switching (no-bifurcation) and bifurcation of vortex rings, respectively. Fig. 8a presents the streamwise (U_{avg}) velocity along the synthetic jet centerline for the bifurcation and no-bifurcation cases. The streamwise velocity component decreases rapidly from the orifice exit to $X/W = 4$ for all the bifurcation cases. This rapid reduction in the streamwise velocity component is linked to the vortex reconnection process, where the counter rotating vortices cancel each other's vorticity leading to a decrease in time-averaged velocity in streamwise direction. After $X/W = 4$, the velocity is negligible as the vortex ring splits and moves away from the synthetic jet centerline (see Fig. 3). On the other hand, in the case of no occurrence of vortex bifurcation, an increase in velocity within the suction zone ($X/W < 3$) is observed. The undulation of velocity in the region between $X/W = 4$ to 9 is related to the axial switching of vortex ring. During the process of axial switching, fluid along the synthetic jet centerline experiences periodic variation in its magnitude.

The cross-stream velocity component (V_{avg}) shown in Fig. 8b is negative (moving towards the synthetic jet centerline) for all the cases in the suction region. The cross-stream velocity increases initially upon moving away from the orifice exit and approaches to zero value near $X/W = 3$ for all bifurcation cases whereas it is positive for all non-bifurcation cases with a peak at $X/W = 4$. This indicates that the suction stroke strongly affects the vortex propagation in downstream direction for bifurcation cases in comparison to that of non-bifurcation cases. At $X/W = 3.5$,

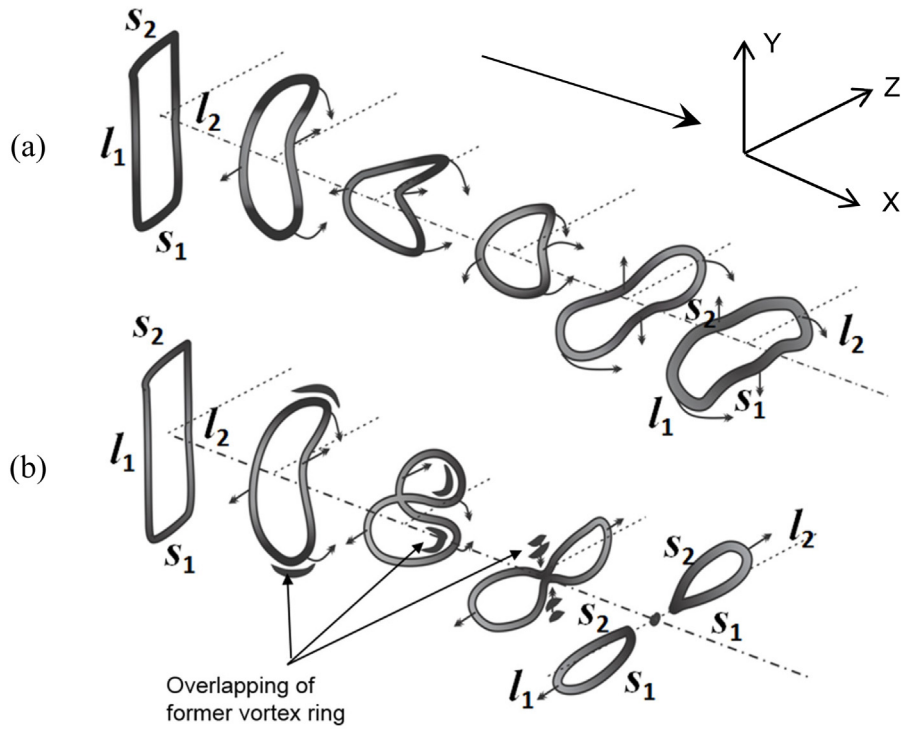

Fig. 7. A schematic comparing the process of (a) axial switching and (b) bifurcation for a rectangular synthetic jet, derived from the current LIF/LDV data and a comparison with the reported study of Kiya et al. [33] for elliptical vortex rings.

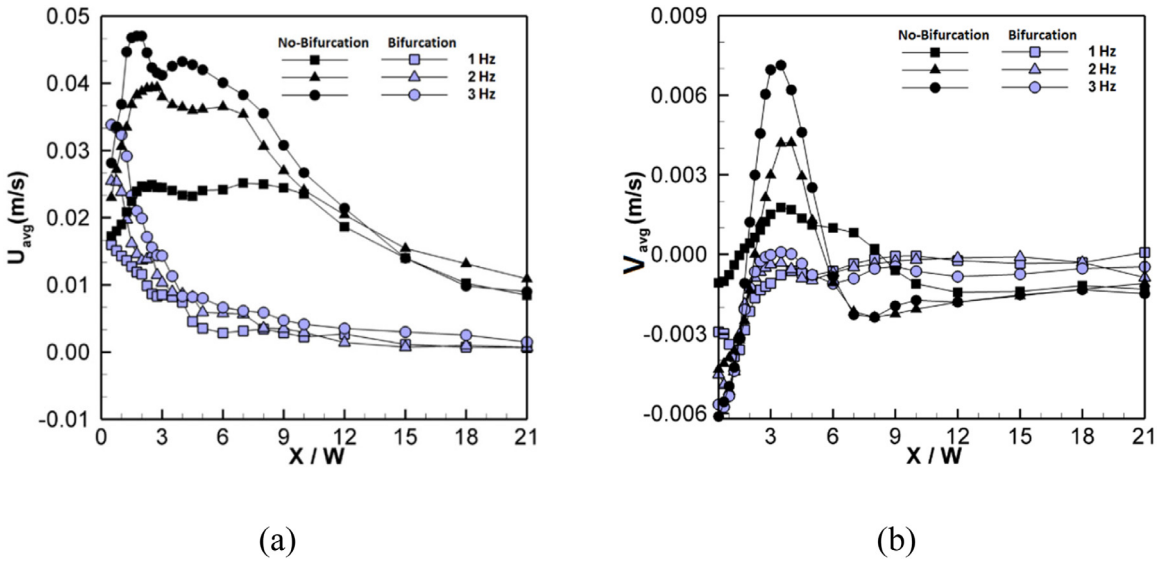

Fig. 8. Time-averaged velocity measurements using LDV for (a) streamwise velocity (U_{avg}) and (b) cross-stream velocity (V_{avg}) along the synthetic jet centerline for all the cases.

where the first axial switching is completed as observed from Fig. 4d, the cross-stream velocity is positive and maximum for non-bifurcation cases but negative or zero for bifurcation cases as seen in Fig. 8b. The positive value of cross-stream velocity at $X/W = 3.5$ for non-bifurcation cases shows that the fluid at the vortex center moves away and prevent the possible reconnection of vortex tube for non-bifurcation cases.

3.5. Different regimes of vortex rings on an Re–St flow map

The range of Reynolds number and Strouhal number for which the rectangular shaped synthetic jet leads to vortex bifurcation under the mentioned experimental conditions are shown in Fig. 9 for a range of actuation frequencies. First, a fixed value of actuation frequency is chosen, and *Re* is varied by changing the magnitude of diaphragm displacement. The resulting average velocity at a particular diaphragm displacement and the actuation frequency fixes the Strouhal number, *St.* Thus, experiments are conducted at all possible values of *Re* and *St* and the range in which vortex bifurcation occurs is recorded. In case of no bifurcation, care has been taken to record the vortex regime — axial switching or vortex suction regime, respectively. It has been observed that the occurrence of vortex bifurcation is crucially dependent upon both *Re* and *St*. The vortex bifurcation cases in

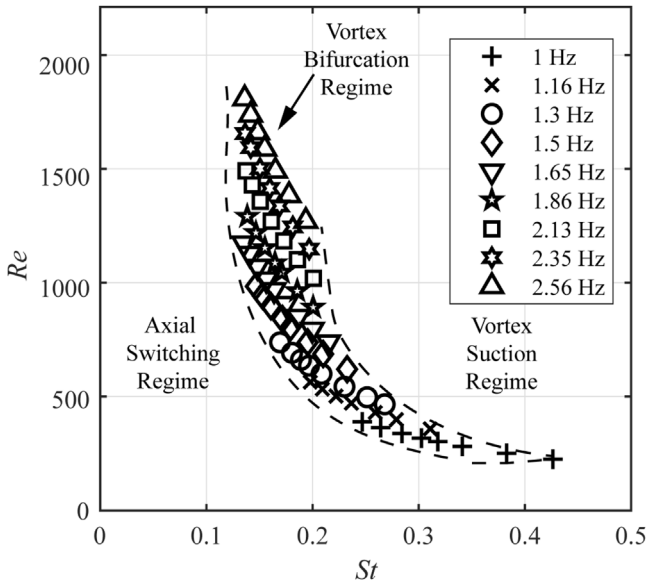

Fig. 9. Different vortex regimes shown on an *Re-St* flow map for AR = 2.

the major axis (*XY*) plane, when plotted on an *Re-St* flow map, falls within a distinctive cornet-like region. To the left of this region, where *St* is low, no distinct vortex splitting is observed and the formed vortex ring undergoes axial switching. And, to its right, exists the vortex suction regime in which there is no distinct formation of vortex ring. In the vortex suction regime, the fluid ejected out from the orifice is sucked back partially or completely inside the cavity during following suction stroke.

4. Conclusions

The bifurcation and axial switching of leading vortex have been studied quantitatively and qualitatively for a rectangular orifice of aspect ratio two. The axial switching and bifurcation of vortex ring are observed and the physical mechanisms behind their occurrence has been proposed using the LIF imaging and the time-averaged velocity measurements. Vortex splitting or bifurcation is observed on the plane coinciding with the minor axis of the orifice. The divergence angles as obtained from LIF images, obtained between the two trajectories of vortex rings are 124° ($Re = 275$, $St = 0.33$) at 1 Hz, 112° ($Re = 1101$, $St = 0.13$) at 2 Hz and 68° ($Re = 1309$, $St = 0.17$) at 3 Hz of actuation frequency. On the other hand, axial switching of vortex ring has been observed at 1, 2 and 3 Hz of actuation frequency for $Re =$ 625, 1348 and 2038 and $St = 0.15$, 0.11 and 0.11 respectively. The main source of bifurcation is believed to be the variation in vortex tube cross section that results in varying self-induced velocity along the length of the vortex tube. When plotted on an *Re-St* flow map, It is observed that the vortex bifurcation regime is a very narrow one between the other regimes such as axial switching and the vortex suction regime.

Declaration of competing interest

The authors declare that they have no known competing financial interests or personal relationships that could have appeared to influence the work reported in this paper.

Acknowledgment

This research was supported by Naval Research Board (NRB), DRDO, Government of India and we thankfully acknowledge their financial assistance.

References

[1] A. Kumar, A. Karn, Qualitative and quantitative characterization of a synthetic jet mounted on a convex torpedo-like surface under cross-flow, Int. J. Heat Fluid Flow 74 (2018) 198–208.
[2] A. Kumar, A. Karn, The effect of a parallel free surface upon a submerged shallow synthetic jet, Fluid Dyn. Res. (2020).
[3] A. Kumar, A. Saha, P. Panigrahi, A. Karn, Implications of velocity ratio on the characteristics of a circular synthetic jet flush mounted on a torpedo model in quiescent and cross-flow conditions, J. Appl. Fluid Mech. 13 (3) (2020).
[4] J.B. Freund, P. Moin, Jet mixing enhancement by high-amplitude fluidic actuation, AIAA J. 38 (10) (2000) 1863–1870.
[5] H. Wang, S. Menon, Fuel-air mixing enhancement by synthetic microjets, AIAA J. 39 (12) (2001) 2308–2319.
[6] M. Amitay, D.R. Smith, V. Kibens, D.E. Parekh, A. Glezer, Aerodynamic flow control over an unconventional airfoil using synthetic jet actuators, AIAA J. 39 (3) (2001) 361–370.
[7] R. Rathnasingham, K.S. Breuer, Active control of turbulent boundary layers, J. Fluid Mech. 495 (2003) 209.
[8] P.S. Krueger, M. Gharib, The significance of vortex ring formation to the impulse and thrust of a starting jet, Phys. Fluids 15 (5) (2003) 1271–1281.
[9] M. Krieg, K. Mohseni, Dynamic modeling and control of biologically inspired vortex ring thrusters for underwater robot locomotion, IEEE Trans. Robot. 26 (3) (2010) 542–554.
[10] S. Gu, S. Guo, L. Zhang, Y. Yao, A hybrid propulsion device for the spherical underwater robot (SUR III), in: 2017 IEEE International Conference on Mechatronics and Automation, ICMA, IEEE, 2017.
[11] C. Wu, N. Ahmed, A preliminary study of the vectoring performance of a synthetic jet actuator with slot edge curvature, Adv. App. Fluid Mech. 15 (2) (2014) 131.
[12] R. Kobayashi, K. Nishibe, Y. Watabe, K. Sato, K. Yokota, Vector control of synthetic jets using an asymmetric slot, J. Fluids Eng. 140 (5) (2018).
[13] L. Huang, Synthetic jet flow and heat transfer for electronics cooling, 2014.
[14] K. Shaikh, S. Kale, A. Kashid, Performance evaluations of synthetic jet cooling for CPU, J. Eng. Technol. (IRJET) (2016) 728–731.
[15] R. Glowienko, H. Derlien, O. Ertunc, A. Delgado, Numerical and experimental analysis of impinging synthetic jets for cooling a point-like heat source, J. Heat Transfer 140 (5) (2018).
[16] A. Pavlova, M. Amitay, Electronic cooling using synthetic jet impingement, 2006.
[17] L.D. Mangate, M.B. Chaudhari, Heat transfer and acoustic study of impinging synthetic jet using diamond and oval shape orifice, Int. J. Therm. Sci. 89 (2015) 100–109.
[18] M.M. Kanase, L.D. Mangate, M.B. Chaudhari, Acoustic aspects of synthetic jet generated by acoustic actuator, J. Low Freq. Noise Vib. Act. Control 37 (1) (2018) 31–47.
[19] Y. Utturkar, R. Holman, R. Mittal, B. Carroll, M. Sheplak, L. Cattafesta, A jet formation criterion for synthetic jet actuators, in: 41st Aerospace Sciences Meeting and Exhibit, 2003.
[20] A. Krothapalli, D. Baganoff, K. Karamcheti, On the mixing of a rectangular jet, J. Fluid Mech. 107 (1981) 201–220.
[21] K. Zaman, Axis switching and spreading of an asymmetric jet: the role of coherent structure dynamics, J. Fluid Mech. 316 (1996) 1–27.
[22] M. Watson, A. Jaworski, N. Wood, A study of synthetic jets from rectangular and dual-circular orifices, Aeronaut. J. 107 (1073) (2003) 427–434.
[23] A. Kumar, A.K. Saha, P.K. Panigrahi, A. Karn, On the flow physics and vortex behavior of rectangular orifice synthetic jets, Exp. Therm Fluid Sci. 103 (2019) 163–181.
[24] L. Wang, L.-H. Feng, J.-J. Wang, T. Li, Parameter influence on the evolution of low-aspect-ratio rectangular synthetic jets, J. Vis. 21 (1) (2018) 105–115.
[25] L. Wang, L.-H. Feng, J.-J. Wang, T. Li, Evolution of low-aspect-ratio rectangular synthetic jets in a quiescent environment, Exp. Fluids 59 (6) (2018) 91.
[26] I. Danaila, B.J. Boersma, Direct numerical simulation of bifurcating jets, Phys. Fluids 12 (5) (2000) 1255–1257.
[27] D. Parekh, A. Leonard, Bifurcating Jets At High Reynolds Numbers, Rep. TF-35, Thermosciences Division, Department of Mechanical Engineering, Stanford University, 1988.
[28] W. Reynolds, D. Parekh, P. Juvet, M. Lee, Bifurcating and blooming jets, Annu. Rev. Fluid Mech. 35 (1) (2003) 295–315.
[29] T.B. Gohil, A.K. Saha, K. Muralidhar, Control of flow in forced jets: a comparison of round and square cross sections, J. Vis. 13 (2) (2010) 141–149.
[30] Y. Oshima, N. Izutsu, K. Oshima, A. Hussain, Bifurcation of an elliptic vortex ring, Fluid Dyn. Res. 3 (1–4) (1988) 133.
[31] S. Iio, T. Kawamura, M. Matsubara, T. Yoshida, T. Ikeda, Vortex behavior of pulsating jets from a rectangular nozzle, JSME Int. J. B 49 (4) (2006) 988–994.

[32] K. Mohseni, Pulsatile vortex generators for low-speed maneuvering of small underwater vehicles, Ocean Eng. 33 (16) (2006) 2209–2223.
[33] M. Kiya, K. Toyoda, H. Ishii, M. Kitamura, T. Ohe, Numerical simulation and flow-visualization experiment on deformation of pseudo-elliptic vortex rings, Fluid Dyn. Res. 10 (2) (1992) 117.
[34] D. Auerbach, T. Grimm, Factors influencing non-circular ring vortex motion, Meccanica 29 (4) (1994) 351–359.
[35] F. Hussain, H.S. Husain, Elliptic jets. Part 1. Characteristics of unexcited and excited jets, J. Fluid Mech. 208 (1989) 257–320.
[36] C.-M. Ho, E. Gutmark, Vortex induction and mass entrainment in a small-aspect-ratio elliptic jet, J. Fluid Mech. 179 (1987) 383–405.
[37] M. Melander, F. Hussain, Cross-linking of two antiparallel vortex tubes, Phys. Fluids A 1 (4) (1989) 633–636.
[38] Z. Yao, S. Xungang, Evolution of single elliptic vortex rings, Acta Mech. Sinica 13 (1) (1997) 17–25.